TABLE I
MEASURED RESULTS OF DUAL-BAND ANTENNA

Frequency (GHz)	2.4	3.5
Bandwidth (%) (VSWR<1.5)	8.7	5.9
Gain (dBi)	1.77	2.17

TABLE II
MEASURED RESULTS OF TRIBAND ANTENNA

Frequency (GHz)	1.8	2.4	3.5
Bandwidth (%) (VSWR<1.5)	21	11	10
Gain (dBi)	1.72	1.53	1.41

the cross-polarization level of H-plane is -13.83 dB at 2.4 GHz and -15.12 dB at 3.5 GHz. The tested gain of the antenna is 1.77 dBi at 2.4 GHz and 2.17 dBi at 3.5 GHz, which is less than the simulated 2.3 dBi.

For triband antennas, the measured and simulated E-plane and H-plane radiation patterns, as well as measured cross polarization of E-plane and H-plane, are shown in Fig. 9. The cross-polarization level of E-plane is -11.92 dB at 1.8 GHz, -11.36 dB at 2.4 GHz, and -11.61 dB at 3.5 GHz. Meanwhile, the cross-polarization level of H-plane is -11.24 dB at 1.8 GHz, -10.12 dB at 2.4 GHz, and -10.78 dB at 3.5 GHz. The tested gain of the antenna is 1.72 dBi at 1.8 GHz, 1.53 dBi at 2.4 GHz, and 1.41 dBi at 3.5 GHz, which is less than the simulated data. The more difference between measurement and simulation on radiation patterns and gain is observed. Because the main current distribution of the frame dipole is along the strip edges, the resonant feature of the frame is sensitive with frame width. That leads to radiation patterns having little distortion when compared to the simulation at each operating frequency and lower gain in test.

Tables I and II show detailed measurement results of dual-band and triband antennas. In general, both dual-band and triband antennas have identical radiation patterns when compared to the traditional strip dipole at each resonant frequency.

V. CONCLUSION

The design of multiband antennas comprising multiple frame-printed dipoles was presented. Two examples of antennas with triband and dual-band characteristics were shown. The structure of multiple frame dipoles offers advantages such as being lightweight, low-cost, simple, and reliable. It has extensive applications for the indoor distribution network of multiband and multimode wireless communication systems, such as DCS, WLAN IEEE 802.11b/g, and WiMax.

REFERENCES

[1] Z. Zhang, M. F. Iskander, J.-C. Langer, and J. Mathews, "Dual-band WLAN dipole antenna using an internal matching circuit," *IEEE Trans. Antennas Propag.*, vol. 53, no. 5, pp. 1813–1818, May 2005.

[2] C. Puente-Baliarda, J. Romeu, R. Pous, and A. Cardama, "On the behavior of the Sierpinski multiband fractal antenna," *IEEE Trans. Antennas Propag.*, vol. 46, no. 4, pp. 517–524, Apr. 1998.

[3] J. Romeu and J. Soler, "Generalized Sierpinski fractal multiband antenna," *IEEE Trans. Antennas Propag.*, vol. 49, no. 8, pp. 1237–1239, Aug. 2001.

[4] C. Puente, J. Romeu, R. Pous, X. Garcia, and F. Benitez, "Fractal multiband antenna based on the Sierpinski gasket," *Electron. Lett.*, vol. 32, no. 1, pp. 1–2, Jan. 1996.

[5] S. R. Best, "A multiband conical monopole antenna derived from a modified Sierpinski gasket," *IEEE Antennas Wireless Propag. Lett.*, vol. 2, pp. 205–207, 2003.

[6] C. T. P. Song, P. S. Hall, and H. Ghafouri-Shiraz, "Multiband multiple ring monopole antennas," *IEEE Trans. Antennas Propag.*, vol. 51, no. 4, pp. 722–729, Apr. 2003.

[7] CST Microwave Studio 2006B. 2006.

Bandwidth Broadening of Dielectric Resonator Antenna by Merging Adjacent Bands

Tze-Hsuan Chang and Jean-Fu Kiang

***Abstract*—A broadband dielectric resonator (DR) antenna is designed by merging its three resonant bands. An asymmetrical moat carved off the DR is designed to perturb the electric field distribution within the DR so that the Q factor of the DR is reduced, and the radiation pattern on the E-plane can be modified to increase the gain in the broadside direction. The mode mixing effect on the radiation patterns is also studied. A wide impedance bandwidth of 33% (4.89–6.86 GHz) is obtained with broadside radiation pattern of vertical polarization on the horizontal plane. This DR antenna can be used for WLAN 802.11a (5.15–5.85 GHz) applications.**

***Index Terms*—Dielectric resonator, resonant mode, mode mixing.**

I. INTRODUCTION

Compared to conventional microstrip antennas, dielectric resonator (DR) antennas can achieve a wider impedance bandwidth due to its larger effective aperture [1]. Radiation pattern of a DR is determined by the field distribution on its surface, hence the former can be modified to some extent by properly trimming the latter.

Different approaches have been proposed to increase the bandwidth of DR antennas, for example, stacking two cylindrical DRs of different sizes to merge their resonant bands [2]–[4], attaching parasitic metal strips on a DR surface to induce additional resonance [5], [6], leaving air gaps between stacked DRs or between a DR and the ground plane to enhance radiation [7]–[9], adjusting the aspect ratio of a DR to reduce its Q factor [10], [11], and so on. Creating structural discontinuities in DRs may also reduce their Q factor, for example, embedding dielectric resonators of different permittivities [4], [12], carving a notch [13], or drilling a series of holes [14].

A wider impedance bandwidth can also be achieved by merging multiple resonant bands [15]–[19]. For example, a truncated tetrahedron with its narrow base attached to the ground plane has a 40% bandwidth in terms of both input impedance and radiation pattern [16]. In [17] and [18], different modes of cylindrical and rectangular DRs with similar broadside radiation patterns are coupled to create a wide bandwidth.

In this work, a rectangular DR with an asymmetrical moat carved off is proposed. The properties of its TE^{y}_{111}, TE^{y}_{112}, and TE^{y}_{113} modes are studied, including their resonant frequencies, radiation patterns, and Q factors. For an intact rectangular DR, the broadside radiation pattern with vertical polarization on the xy-plane associated with TE^{y}_{112} mode is quite different from those of TE^{y}_{111} and TE^{y}_{113} modes. By properly

Manuscript received March 20, 2008; revised March 27, 2009. First published August 11, 2009; current version published October 07, 2009. This work was supported by the National Science Council, Taiwan, ROC, under Contract NSC 95-2221-E-002-085.

The authors are with the Department of Electrical Engineering and the Graduate Institute of Communication Engineering, National Taiwan University, Taipei, Taiwan (e-mail: jfkiang@cc.ee.ntu.edu.tw).

Digital Object Identifier 10.1109/TAP.2009.2029372

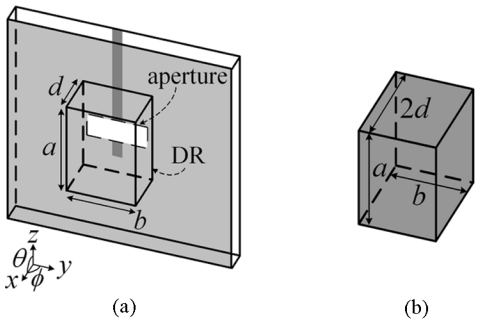

Fig. 1. (a) DR on a ground plane. (b) Equivalent DR in free space.

merging the resonant bands of TE^{y}_{111}, TE^{y}_{112}, and TE^{y}_{113} modes, a wide bandwidth can be acquired in terms of return loss and radiation pattern.

II. Resonant Modes of Rectangular DRs

Fig. 1(a) shows a rectangular DR of dimensions $a \times b \times d$ placed on a ground plane, which is equivalent to an isolated DR of dimensions $a \times b \times 2d$ in free space, as shown in Fig. 1(b). The resonant frequencies of TE modes in a rectangular DR can be predicted with reasonable accuracy using the dielectric waveguide model [20]. In this model, fields are assumed totally reflected by two opposite sides of the DR, while the other four sides behave like PMC walls. The resonant frequencies of the TE^{y}_{11m} modes can thus be estimated as $f_r = c\sqrt{k_x^2 + k_y^2 + k_z^2}/\sqrt{\epsilon_r}$, where $k_x = \pi/2d, k_z = m\pi/a$, and $k_y = 2\tan^{-1}(\sqrt{k_x^2 + k_z^2}/k_y)/b$ [21].

The radiation field can be derived from the equivalent surface currents $\bar{J}_s$ and $\bar{M}_s$ on the DR surface. Similar broadside radiation pattern with maximum E_θ at $\theta = 90^\circ$ is generated when TE^{y}_{111} or TE^{y}_{113} mode is excited. A broad bandwidth can be acquired if the frequency bands of these two modes can be merged [17], [18]. However, there remains one obstacle, the E_θ pattern radiated by exciting the TE^{y}_{112} mode, of which the resonant frequency lies between those of the above two and has a null at $\theta = 90^\circ$.

We first check how the aspect ratios affect the resonant frequencies of the three modes that will be involved in the design. Fig. 2(a) shows the resonant frequencies of these three modes at different aspect ratios, with $b = 9$ mm. When the ratio a/b is increased, the resonant frequencies of these three modes decrease at different rates and become closer at large a/b ratio. As the d/b ratio is increased, the difference among three resonant frequencies becomes large, which implies that merging the resonant bands of the three modes is easier with small d/b ratio. To provide another perspective, Fig. 2(b) shows the ratios of resonant frequencies of TE^{y}_{112} and TE^{y}_{113} modes with respect to that of TE^{y}_{111} mode.

We also check the Q factors of these three modes, as shown in Fig. 3(a). The Q factor of TE^{y}_{111} mode is on the order of 10, reaches a maximum at $a \simeq b$, and is slightly affected by the d/b ratio. The Q factor of TE^{y}_{112} mode ranges between 10 and 100, and decreases as d/b is increased. The Q factor of TE^{y}_{113} mode ranges from 100 to 10 000 and dramatically increases around different a/b ratios at different d/b ratios. Fig. 3(b) shows the effect of DR permittivity on the Q factors of two different DR dimensions. The Q factor increases smoothly when the permittivity is increased.

III. Effect of DR Shape Modification

The Q factor of a DR antenna can be reduced by leaving a gap or carving a notch at the bottom of the DR, causing the power to be radiated more effectively [9], [23]. In [14], a well is carved off a DR

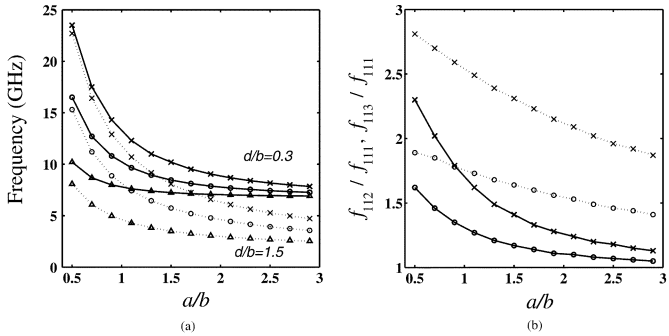

Fig. 2. (a) Resonant frequencies at different d/b ratios given a/b ratio. (b) Ratios of resonant frequencies of TE^{112}_{y} and TE^{113}_{y} modes with respect to that of TE^{111}_{y} mode. —: $d/b = 0.3$; ... : $d/b = 1.5$, △ : TE^{y}_{111} mode; ∘ : TE^{y}_{112} mode; × : TE^{y}_{113} mode; $\epsilon_r = 20$; $b = 9$ mm.

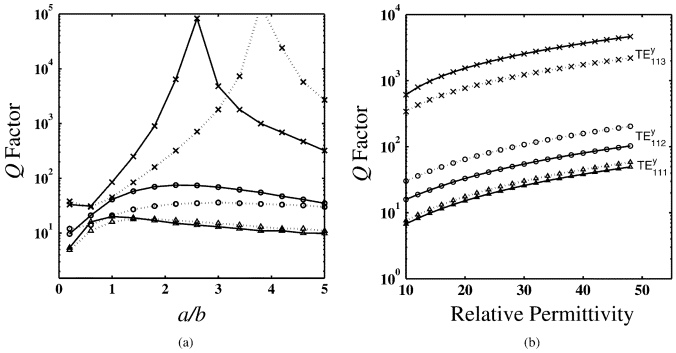

Fig. 3. (a) Q factors at different d/b ratios given a/b ratio. —: $d/b = 0.5$; ... : $d/b = 1$; $\epsilon_r = 20$; $b = 9$ mm. (b) Q factors at different permittivities. $b = 9$ mm; —: $a/b = 3.1$; $d/b = 1.1$; ... : $a/b = 1.89$; $d/b = 0.56$; △ : TE^{y}_{111}; ∘ : TE^{y}_{112}; × : TE^{y}_{113}.

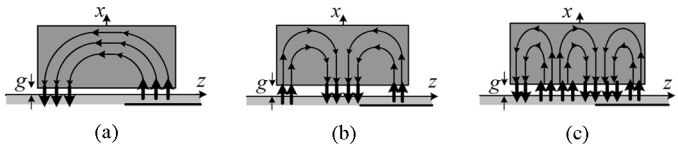

Fig. 4. Electric field distribution within gap and DR: (a) TE^{y}_{111} mode, (b) TE^{y}_{112} mode, (c) TE^{y}_{113} mode.

and filled with low-permittivity materials; the electric field distribution within the well is significantly enhanced, hence the Q factor is significantly reduced. In this section, we will analyze the effects of a gap and two asymmetrical wells on the resonant frequencies and radiation patterns of the DR.

A. Effect of Gap

When a gap appears between the DR and its ground plane, the electric field within the gap is normal to the ground plane and is amplified due to continuity of electric flux density across the dielectric-air interface, as shown in Fig. 4. If the gap height g is small, the electric field distribution of TE^{y}_{11m} mode within the gap can be approximated as

$$E_{0x} \simeq -m_1 k_z A \cos(k_y y)\sin(k_z z) \tag{1}$$

for odd m, or

$$E_{0x} \simeq m_2 k_z B \cos(k_y y)\cos(k_z z) \tag{2}$$

for even m, where m_1 and m_2 are the amplification factors comparing the electric fields in the gap and in the DR. These factors are close to the relative dielectric constant of the DR. By substituting the perturbed

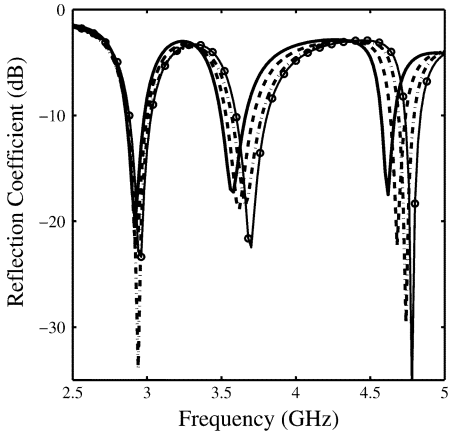

Fig. 5. Effect of gap between DR and ground plane; $\epsilon_r = 20$, $a = 28$ mm, $b = 9$ mm, $d = 10$ mm, $L_s = 6$ mm, $d_s = 7$ mm, $L_a = 10$ mm, $w_a = 2$ mm, $W_g = L_g = 60$ mm, —: $g = 0$ mm, - - -: $g = 0.01$ mm, -·-: $g = 0.02$ mm, -o-: $g = 0.03$ mm.

TABLE I
COMPARISON OF RESONANT FREQUENCY SHIFT AT DIFFERENT GAP HEIGHTS. FREQUENCY IN GHZ, LENGTH IN MM

$f_r(\Delta f)$	$g = 0$	$g = 0.01$	$g = 0.02$	$g = 0.03$
HFSS	2.92	2.93 (0.01)	2.94 (0.02)	2.95 (0.03)
Theory (TE^y_{111})	2.828	2.84 (0.011)	2.85 (0.022)	2.862(0.033)
HFSS	3.57	3.61 (0.04)	3.66 (0.09)	3.69 (0.12)
Theory (TE_{112})	3.66	3.685(0.026)	3.71 (0.05)	3.74 (0.08)
HFSS	4.62	4.68 (0.06)	4.74 (0.12)	4.78 (0.16)
Theory (TE^y_{113})	4.648	4.688(0.04)	4.728(0.08)	4.767(0.12)

electric field distributions of (1) or (2) into the reaction formula, resonant frequencies of the modified DR structure can be estimated with reasonable accuracy [25].

As shown in Fig. 5, the resonant frequencies of all the three modes increase with increasing g. Table I lists the comparison of resonant frequency shift to simulation and to reaction formulas, respectively. It is also observed that the radiation pattern is hardly affected by the gap.

B. Effect of Two Asymmetric Wells

Fig. 6(a) shows a DR antenna with two wells of dimensions $s_1 \times s_2 \times d$ and $s_3 \times s_4 \times d$, respectively, and they are located away from the DR center by l_1 and l_2, respectively. The electric field distribution within the otherwise intact DR is significantly perturbed by the two wells, and HFSS is used to estimate the resonant frequencies.

The electric field polarizations of the TE^y_{112} mode are opposite on two sides of the DR top surface since $E_z \propto \sin(\pi z/a)$, thus producing a null of E_θ radiation pattern in the x direction. By adjusting the size and position of the two wells to break the symmetry of E_z, the E_θ radiation pattern will be tilted, rendering a higher gain in the xy-plane.

Fig. 7(a) and (b) show the simulated reflection coefficient and E_θ patterns in the xz-plane, respectively. When s_3 is decreased from 2 to 0.5 mm, the null direction shifts from $\theta = -3^\circ$ to $\theta = -15^\circ$, resulting in a gain increase of E_θ pattern in the x direction from -12 to -3 dBi.

IV. MODE MIXING

The bandwidth of a DR antenna can be increased by merging bands of different modes [15]–[19]. In this work, the bands associated with

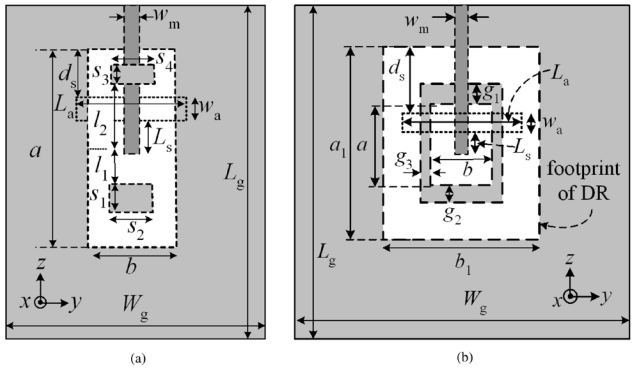

Fig. 6. (a) Configuration of DR antenna embedded with two asymmetric wells. (b) DR antenna with a moat and feed network.

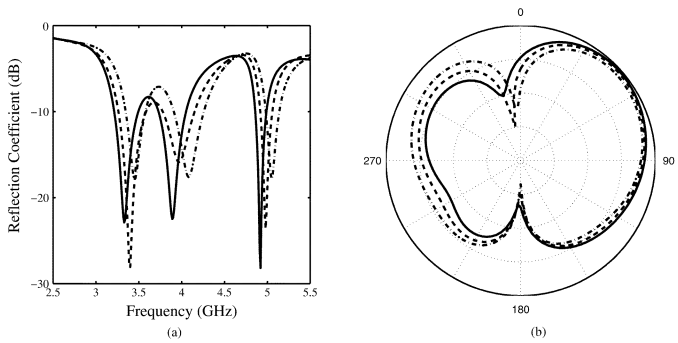

Fig. 7. Effect of two asymmetric wells on (a) reflection coefficient and (b) radiation patterns; $\epsilon_r = 20$, $a = 28$ mm, $b = 9$ mm, $d = 10$ mm, $s_2 = s_4 = 7$ mm, $s_1 = 2$ mm, $L_s = 6$ mm, $d_s = 7$ mm, $L_a = 10$ mm, $w_a = 2$ mm, $W_g = L_g = 60$ mm, —: $s_3 = 0.5$ mm, - - -: $s_3 = 1$ mm, -·-: $s_3 = 2$ mm.

the TE^y_{111} and TE^y_{113} modes are merged to broaden the bandwidth over which the radiation patterns in the xy-plane look similar. Based on previous discussion, DRs with a lower profile have closer resonant frequencies of TE^y_{111} and TE^y_{113} modes. However, the TE^y_{112} mode generates a quite different radiation pattern, and its resonant frequency sits between those of the TE^y_{111} and TE^y_{113} modes. At frequencies between the resonant frequencies f_{111} (of TE^y_{111} mode) and f_{112} (of TE^y_{112} mode), the electromagnetic field in the DR can be decomposed as $\bar{E}_t = \bar{E}_{111} + \alpha e^{j\xi}\bar{E}_{112}$ and $\bar{H}_t = \bar{H}_{111} + \alpha e^{j\xi}\bar{H}_{112}$, where α and ξ are relative magnitude and phase difference, respectively. The radiation pattern is also contributed by these two modes in the same proportions.

Consider a rectangular DR of dimensions 29 mm × 19 mm × 4 mm. The resonant frequency f_r, radiation quality factor Q_{rad}, and gain G_{D} are listed in Table II. The gain associated with TE^y_{113} mode is higher than that with TE^y_{111} mode. In other words, the beamwidth associated with TE^y_{113} mode is narrower than that with TE^y_{111} mode.

The input impedance can be matched, and bands of the three modes can be merged to achieve an impedance bandwidth of 25%, as shown in Fig. 8(a). Fig. 8(b) shows that the gain reaches a minimum around $f = 4.81$ GHz, close to the resonant frequency of TE^y_{112} mode. The gain variation over the impedance bandwidth is about 5 dB. Note that this minimum gain is apparently larger than that associated with the TE^y_{112} mode alone due to the compensation by TE^y_{111} and TE^y_{113} modes. By lowering the DR profile, the resonant frequencies f_{111} and f_{113} move closer to f_{112}, and the gain with the TE^y_{112} mode in the xy-plane is thus increased. If the DR profile is raised, its impedance bandwidth becomes wider, but its gain variation is also increased.

TABLE II
COMPARISON OF RESONANT FREQUENCY f_r, $Q_{\rm rad}$, AND DIRECTIVITY G_D OF RESONANT MODES

Modes	f_r (GHz)	$Q_{\rm rad}$	$G_D(\theta = 90^\circ, \phi = 0^\circ)$ (dBi)
TE^y_{111}	4.56	10.5	5.84
TE^y_{112}	4.96	117	$-\infty$
TE^y_{113}	5.56	2,272	8.43

All parameters are the same as in Fig. 8.

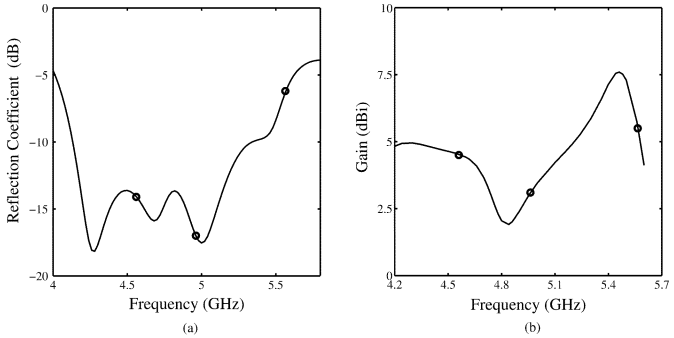

Fig. 8. (a) Simulated reflection coefficient and (b) gain of E_θ pattern at $\theta = 90^\circ$, $\epsilon_r = 20$, $a = 30$ mm, $b = 19$ mm, $d = 4$ mm, $d_s = 12$ mm, $w_a = 1$ mm, $L_a = 7$ mm, $L_s = 4$ mm, $W_g = L_g = 70$ mm; $\circ$ marks the resonant frequencies of TE^y_{111}, TE^y_{112}, and TE^y_{113} modes, respectively.

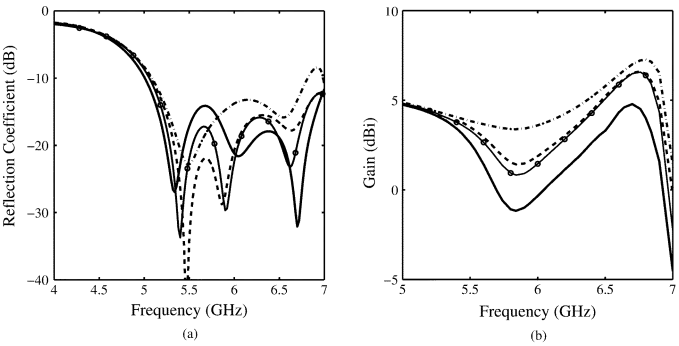

Fig. 9. Effect of d_s on (a) reflection coefficient and (b) gain at $\theta = 90^\circ$ and $\phi = 0^\circ$, —: $d_s = 12$ mm, - - -: $d_s = 13$ mm, -·-: $d_s = 14$ mm, -o-: $d_s = 16$ mm, $\epsilon_r = 20$,$a = 17$ mm, $b = 10$ mm, $a_1 = 30.5$ mm, $b_1 = 19$ mm, $d = 4$ mm, $g_1 = g_2 = 2.75$ mm, $g_3 = 0.5$ mm, $L_s = 4$ mm, $L_a = 12$ mm, $w_a = 2$ mm, $W_g = L_g = 70$ mm.

V. RECTANGULAR DR WITH MOAT

Fig. 6(b) shows a DR antenna with an asymmetric moat. The gap widths are marked as g_1, g_2, and g_3, respectively. Fig. 9 shows the effect of feeding parameter d_s on the input impedance and gain. The gain decreases to -1 dBi at 5.84 GHz when d_s is 12 mm, increases to 3.8 dBi when d_s is 14 mm, and slightly decreases to 1 dBi as d_s becomes longer. It appears that the position of coupling aperture affects the composition of the resonant modes.

Fig. 10(a) shows the effect of air gaps g_1 and g_2 on the gain. When the gap is large, radiation becomes more effective, hence the Q factor is decreased and the impedance bandwidth is increased. When g_1 and g_2 are made asymmetric, say g_1 is small and g_2 is large, the gain variation over 4.5–6.4 GHz is about 1.8 dB. When g_1 is further increased and g_2 decreased, the gain drops near f_{112}, and the gain variation becomes 4.8 dB. It appears that g_1 and g_2 can be used to adjust the E_z distribution of the TE^y_{112} mode within the DR.

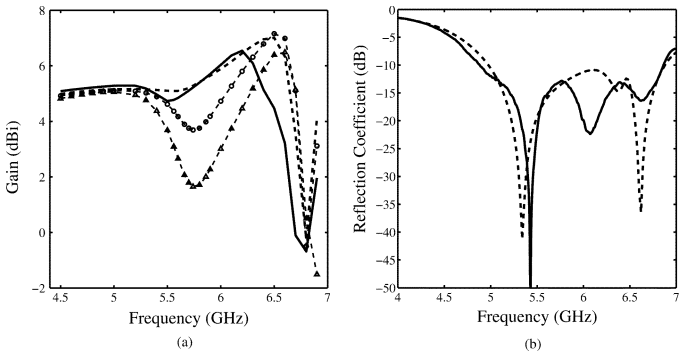

Fig. 10. (a) Effect of g_1 on gain of E_θ pattern at $\theta = 90^\circ$ and $\phi = 0^\circ$, —: $g_1 = 0.1$ mm, $g_2 = 5.3$ mm, - - -: $g_1 = 0.2$ mm, $g_2 = 5.2$ mm, -o-: $g_1 = 1$ mm, $g_2 = 4.4$ mm, -△-: $g_1 = 2$ mm, $g_2 = 3.4$ mm, $\epsilon_r = 20$, $a = 16.5$ mm, $b = 10$ mm, $a_1 = 30$ mm, $b_1 = 19$ mm, $d = 4$ mm, $L_s = 5$ mm, $d_s = 13$ mm, $g_3 = 0.2$ mm, $L_a = 13.5$ mm, $w_a = 2$ mm, $W_g = L_g = 70$ mm, (b) reflection coefficient, —: measurement, - - -: simulation, all parameters are the same as (a), except $a_2 = 30.5$ mm, $d_s = 12.5$ mm and $g_1 = 0.5$ mm.

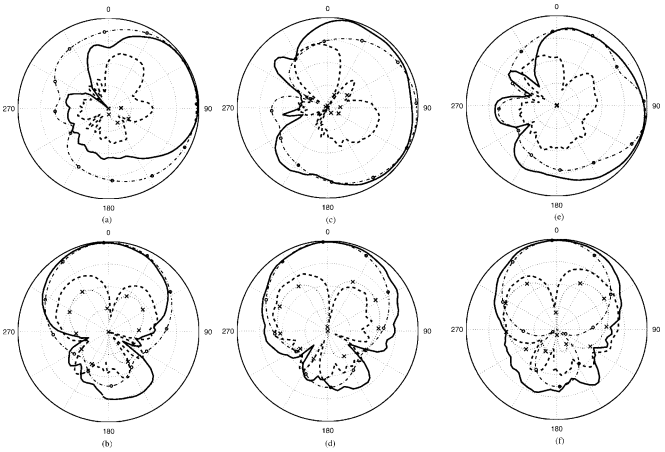

Fig. 11. Radiation patterns (a) in xz-plane at $f = 5.5$ GHz, (b) in xy-plane at $f = 5.5$ GHz, (c) in xz-plane at $f = 6$ GHz, (d) in xy-plane at $f = 6$ GHz, (e) in xz-plane at $f = 6.6$ GHz, (f) in xy-plane at $f = 6.6$ GHz; —: measured E_θ, - - -: measured E_ϕ, $-\circ-$: simulated E_θ, -×-: simulated E_ϕ, 10-dB per division on radials, all parameters are the same as in Fig. 10(b).

By properly tuning g_1, g_2, and d_s, a wide impedance bandwidth with acceptable gain variation can be acquired. Fig. 10(b) shows the measured and simulated reflection coefficient, which match reasonably well. The 10-dB input-impedance bandwidth is about 33% (4.89–6.86 GHz), covering the WLAN 802.11a band (5.15–5.85 GHz). Without the moat, the band will shift to lower frequencies, and the bandwidth is only about 25%.

Fig. 11 shows the radiation patterns in the xz- and xy-planes, respectively. At $f = 5.5$ GHz, close to f_{111}, the half-power beamwidth (HPBW) of E_θ pattern in the xy-plane is about 75° ($-35^\circ \le \phi \le 40^\circ$), with cross polarization (E_ϕ) lower by 9 dB. The front-to-back ratio is 10 dB, and the gain is 5.3 dBi. For WLAN applications, for example, this DR antenna can be mounted on wall with the z-axis pointing to ceiling, thus providing a broadside radiation pattern with vertical polarization in the xy-plane in front of the wall.

At $f = 6$ GHz, close to f_{112}, the HPBW of E_θ pattern in the xy-plane is about 83° ($-43^\circ \le \phi \le 40^\circ$), with cross polarization lower by 9 dB. The gain is 3 dBi, and the front-to-back ratio is about 15 dB.

At $f = 6.6$ GHz, close to f_{113}, the HPBW of E_θ pattern in the xy-plane is about 80° ($-40^\circ \leq \phi \leq 40^\circ$), with cross polarization lower by 7 dB. The gain is 4.3 dBi and the front-to-back ratio is about 12 dB.

VI. Conclusion

The radiation pattern, radiation Q factor, and gain of rectangular DRs embedded with wells or moat are analyzed. The mixing of TE^y_{111}, TE^y_{112}, and TE^y_{113} modes is exploited to extend the bandwidth of radiation pattern. The resonant bands associated with these modes are merged to design a DR antenna with a broad bandwidth in input impedance and radiation pattern. Its 10-dB bandwidth is about 33% (4.89–6.86 GHz) with broadside radiation pattern, which covers the WLAN 802.11a band.

References

[1] S. A. Long, M. W. Mcallister, and L. C. Shen, "The resonant cylindrical dielectric cavity antenna," *IEEE Trans. Antennas Propag.*, vol. AP-31, no. 3, pp. 406–412, May 1983.

[2] A. A. Kishk, B. Ahn, and D. Kajfez, "Broadband stacked dielectric resonator antenna," *Electron. Lett.*, vol. 25, no. 18, pp. 1232–1233, Aug. 1989.

[3] Q. Rao, T. A. Denidi, and A. R. Sebak, "Broadband compact stacked T-shaped DRA with equilateral-triangular cross sections," *IEEE Microw. Wireless Comp. Lett.*, vol. 16, no. 1, pp. 7–9, Jan. 2006.

[4] A. G. Walsh, C. S. De Young, and S. A. Long, "An investigation of stacked and embedded cylindrical dielectric resonator antennas," *IEEE Antennas Wireless Propag. Lett.*, vol. 5, pp. 130–133, 2006.

[5] F. R. Hsiao, C. Wang, K. L. Wong, and T. W. Chiou, "Broadband very-high-permittivity dielectric resonator antenna for WLAN application," in *Proc. IEEE APS Int. Symp.*, Jun. 2002, vol. 4, pp. 490–493.

[6] K. W. Leung and H. K. Ng, "The slot-coupled hemispherical dielectric resonator antenna with a parasitic patch: Applications to the circularly polarized antenna and wide-band antenna," *IEEE Trans. Antennas Propag.*, vol. 53, no. 5, pp. 1762–1769, May 2005.

[7] S. M. Shum and K. M. Luk, "Characteristics of dielectric ring resonator antenna with an air gap," *Electron. Lett.*, vol. 30, no. 4, pp. 277–278, Feb. 1994.

[8] S. M. Shum and K. M. Luk, "Stacked annular ring dielectric resonator antenna excited by axi-symmetric coaxial probe," *IEEE Trans. Antennas Propag.*, vol. 43, no. 8, pp. 889–890, Aug. 1995.

[9] Y.-X. Guo, Y.-F. Ruan, and X.-Q. Shi, "Wide-band stacked double annular-ring dielectric resonator antenna at the end-fire mode operation," *IEEE Trans. Antennas Propag.*, vol. 53, no. 10, pp. 3394–3397, Oct. 2005.

[10] R. K. Mongia, A. Ittipiboon, P. Bhartia, and M. Cuhaci, "Electric-monopole antenna using a dielectric ring resonator," *Electron. Lett.*, vol. 29, no. 17, pp. 1530–1531, Aug. 1993.

[11] M. Verplanken and J. V. Bladel, "The magnetic-dipole resonances of ring resonators of very high permittivity," *IEEE Trans. Microw. Theory Tech.*, vol. MTT-27, no. 4, pp. 328–333, Apr. 1979.

[12] A. A. Kishk, "Experimental study of broadband embedded dielectric resonator antennas excited by a narrow slot," *IEEE Antennas Wireless Propag. Lett.*, vol. 4, pp. 79–81, 2005.

[13] A. Ittipiboon, A. Petosa, D. Roscoe, and M. Cuhaci, "An investigation of a novel broadband dielectric resonator antenna," in *Proc. IEEE APS Int. Symp.*, Jul. 1996, vol. 3, pp. 2038–2041.

[14] R. Chair, A. A. Kishk, and K. F. Lee, "Experimental investigation for wideband perforated dielectric resonator antenna," *Electron. Lett.*, vol. 42, no. 3, pp. 137–138, Feb. 2006.

[15] A. A. Kishk, Y. Yan, and A. W. Glisson, "Conical dielectric resonator antennas for wide-band applications," *IEEE Trans. Antennas Propag.*, vol. 50, no. 4, pp. 469–474, Apr. 2002.

[16] A. A. Kishk, "Wide-band truncated tetrahedron dielectric resonator antenna excited by a coaxial probe," *IEEE Trans. Antennas Propag.*, vol. 51, no. 10, pp. 2913–2917, Oct. 2003.

[17] R. Chair, A. A. Kishk, and K. F. Lee, "Wideband simple cylindrical dielectric resonator antennas," *IEEE Microw. Wireless Comp. Lett.*, vol. 15, no. 4, pp. 241–243, Apr. 2005.

[18] C. S. Deyoung and S. A. Long, "Wideband cylindrical and rectangular dielectric resonator antennas," *IEEE Antennas Wireless Propag. Lett.*, vol. 5, pp. 426–429, 2006.

[19] B. Li and K. W. Leung, "Strip-fed rectangular dielectric resonator antennas with/without a parasitic patch," *IEEE Trans. Antennas Propag.*, vol. 53, no. 7, pp. 2200–2207, Jul. 2005.

[20] R. K. Mongia, "Theoretical and experimental resonant frequencies of rectangular dielectric resonators," *Proc. Microw., Antennas, Propag.*, vol. 139, no. 1, pp. 98–104, Feb. 1992.

[21] Y. M. M. Antar, D. Cheng, G. Seguin, B. Henry, and M. G. Keller, "Modified waveguide model (MWGM) for rectangular resonator antenna (DRA)," *Microw. Opt. Tech. Lett.*, vol. 19, no. 2, pp. 158–160, Oct. 1998.

[22] R. K. Mongia and A. Ittipiboon, "Theoretical and experimental investigations on rectangular dielectric resonator antennas," *IEEE Trans. Antennas Propag.*, vol. 45, no. 9, pp. 1348–1356, Sep. 1997.

[23] Y.-D. Kim, M.-S. Kim, and H.-M. Lee, "Internal rectangular dielectric resonator antenna with broadband characteristic for IMT-2000 handset," in *Proc. IEEE APS Int. Symp.*, Jun. 2002, vol. 3, pp. 22–25.

[24] R. Chair, A. A. Kishk, and K. F. Lee, "Wideband low profile eye shaped dielectric resonator antennas," in *Proc. IEEE APS Int. Symp.*, Jul. 2005, vol. 3A, pp. 582–585.

[25] T.-H. Chang and J.-F. Kiang, "Dualband split dielectric resonator antenna," *IEEE Trans. Antennas Propag.*, vol. 55, no. 11, pp. 3155–3162, Nov. 2007.